AGU PUBLICATIONS

Geophysical Research Letters

RESEARCH LETTER
10.1002/2015GL064985

Key Points:
- Relic arcs adjacent to a plate interface is a favorable place for spontaneous subduction initiation
- Both temperature and composition effects at relic arcs contribute as driving mechanism
- Passive margins tend to be stable because of negative temperature contribution

Supporting Information:
- Table S1

Correspondence to:
W. Leng,
wleng@ustc.edu.cn

Citation:
Leng, W., and M. Gurnis (2015), Subduction initiation at relic arcs, *Geophys. Res. Lett.*, *42*, 7014–7021, doi:10.1002/2015GL064985.

Received 18 JUN 2015
Accepted 11 AUG 2015
Accepted article online 14 AUG 2015
Published online 5 SEP 2015

Subduction initiation at relic arcs

Wei Leng[1,2] and Michael Gurnis[3]

[1]Laboratory of Seismology and Physics of Earth's Interior, School of Earth and Space Sciences, University of Science and Technology of China, Hefei, China, [2]National Geophysical Observatory at Mengcheng, Mengcheng, China, [3]Seismological Laboratory, California Institute of Technology, Pasadena, California, USA

Abstract Although plate tectonics is well established, how a new subduction zone initiates remains controversial. Based on plate reconstruction and recent ocean drilling within the Izu-Bonin-Mariana, we advance a new geodynamic model of subduction initiation (SI). We argue that the close juxtaposition of the nascent plate boundary with relic oceanic arcs is a key factor localizing initiation of this new subduction zone. The combination of thermal and compositional density contrasts between the overriding relic arc, and the adjacent old Pacific oceanic plate promoted spontaneous SI. We suggest that thermal rejuvenation of the overriding plate just before 50 Ma caused a reduction in overriding plate strength and an increase in the age contrast (hence buoyancy) between the two plates, leading to SI. The computational models map out a framework in which rejuvenated relic arcs are a favorable tectonic environment for promoting subduction initiation, while transform faults and passive margins are not.

1. Introduction

Slab pull has long been recognized as the fundamental force driving plate tectonics [*Forsyth and Uyeda*, 1975; *Hager and O'Connell*, 1981], but the process by which new subduction zones initiate remains subject to debate from both observational and geodynamic perspectives. The Izu-Bonin-Mariana (IBM) subduction zone—with the locus of initiation identified (the Kyushu-Palau Ridge, KPR, Figure 1a), subsequent evolution resolved, and initiation age (~52–50 Ma) constrained within 1 Ma through study of the fore arc [*Cosca et al.*, 1998; *Ishizuka et al.*, 2011a]—has become the archetypical region to frame our understanding of subduction initiation (SI). Geodynamic interpretations for IBM have posited that the initiation occurred along an existing fracture zone through either spontaneous [*Stern and Bloomer*, 1992] or compression-induced [*Hall et al.*, 2003] mechanisms. However, IBM initiation at an old fracture zone has been questioned [*Taylor and Goodliffe*, 2004] because (1) the spreading responsible for the generally orthogonal relation between the KPR and spreading fabric to the west of KPR postdates the age of initiation and (2) the initial site of SI cuts across preexisting fabric on the overriding plate (best shown for the Amami Sankaku Basin, ASB, region, Figure 1b). With the elevated importance of IBM, recent ocean drilling has focused on the region with International Ocean Discovery Program (IODP) Expedition 351 targeting the basement and sediment cover of the overriding plate adjacent to the KPR and Expedition 352 targeting the Bonin fore-arc section to decipher the early volcanic stratigraphy. The results of these expeditions are upending existing scenarios for IBM initiation and call for a new evaluation of the geodynamics of subduction initiation.

There are several fundamental discoveries from the recent drilling. First, the age of the basement (ASB, Figure 1b) is not Cretaceous as commonly thought [*Seton et al.*, 2012], but 57–50 Ma [*Expedition 351 Scientists*, 2014], and hence overlapping the age of initiation inferred from rocks recovered on the IBM fore arc. Consequently, at initiation the basement of the overriding plate was quite young and its age may have even been close to zero. Geochemical analysis of the basement indicates that the mantle source was highly depleted and that the mantle source may have already interacted with a subducting plate [*Arculus et al.*, 2015]. Together with ages of the surrounding region [*Ishizuka et al.*, 2011b], a pervasive east west tectonic fabric between the Amami Plateau and the Daito Ridge [cf. *Ishizuka et al.*, 2011b, Figure 1c] suggests rapid extension of the overriding plate orthogonal to the new IBM subduction zone.

In addition, we believe that the importance of the preexisting Amami Plateau, Daito Ridge, and Oki-Daito Ridge (Figures 1a and 1b) have been underestimated when evaluating the importance of the different geodynamic factors that lead to subduction initiation. The Amami Plateau, Daito Ridge, and Oki-Daito Ridge are clearly Cretaceous with radiometric ages of recovered samples of andesites, basalts, tonolites, gabbros, and

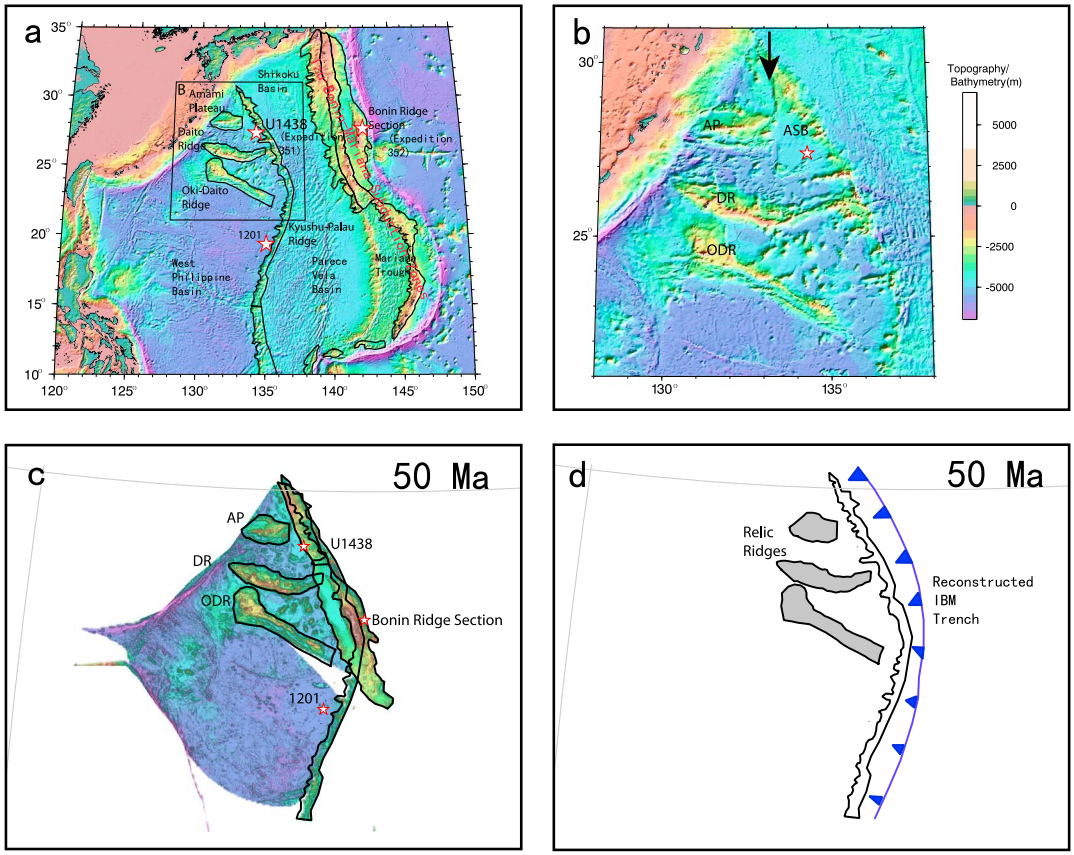

Figure 1. (a) Basemap of the Philippine Sea Plate using the location of recent drilling at Site U1438 (Expedition 351) and the Bonin Ridge section encompassing in Sites U1439 to U1442 (Expedition 352) and the earlier work of *Ishizuka et al.* [2011a]. Also indicated with black lines are the relic arcs, including the site of subduction initiation, the Kyushu-Palau Ridge (KPR), and existing drill site 1201. (b) Zoom in of the region around U1438, the ASB (Amami Sankaku Basin) and the relic ridges AP (Amami Plateau), DR (Daito Ridge), and the ODR (Oki-Daito Ridge). The black vertical arrow locates the linear fault, presumed transform fault, or fracture zone which defines the western boundary of the ASB. The star is Site U1438. Scale for Figures 1a and 1b is shown. (c) Reconstruction at 50 Ma of the present-day topography using the poles of rotation in *Seton et al.* [2012]. (d) Outlines of the relic arcs (in grey shading) from Figure 1c indicated, along with the approximate location of the new trench (in blue) at 50 Ma. For Figures 1a–1c, the bathymetry version 18.1 of *Smith and Sandwell* [1997] is used.

granites ranging in age from 110 to 160 Ma [*Hickey-Vargas*, 2005; *Ishizuka et al.*, 2011b]. The basement is capped with middle Eocene sediments indicative of subsequent subsidence and cooling of the inactive arcs [*Mizuno et al.*, 1978]. Using rotations for the opening of the Mariana Trough and the Shikoku, Parece Vela, and West Philippine basins [*Seton et al.*, 2012], we reconstruct the Izu and Bonin Ridges to 50 Ma—the age of subduction initiation (Figure 1c). We find the IBM fore arc is adjacent to these three relic arcs (Figures 1c and 1d). This simple reconstruction points to a much smaller overriding plate [*Deschamps and Lallemand*, 2002] in which the relic arcs existed along a substantial length of the newly forming plate margin.

The crustal structure of these relic arcs has been determined with recent, transecting seismic refraction lines. Differing from normal oceanic plates with an ~7 km thick crust, the lines show that the ridges have lower seismic velocities and crustal thicknesses of 15–25 km, similar to the more geologically recent Mariana arcs [*Nishizawa et al.*, 2014]. Detailed interpretations have been made of the seismic structure at the analogous Mariana arc in which the thickness and composition of the arc upper crust is similar to the basaltic oceanic crust but that the density of the middle and lower arc crust is significantly lower than the oceanic upper mantle (Figures 2a and 2b) [*Takahashi et al.*, 2007]. Taking the Izu-Bonin arc as an example, petrological studies suggest that the middle and lower arc crust is mostly composed of tonalite and gabbro, with densities of ~2700 kg/m^3 and ~2900 kg/m^3, respectively [*Kitamura et al.*, 2003]. This suggests a density contrast of 12–18% compared with the oceanic upper mantle (~3300 kg/m^3) (Figure 2c). This conclusion

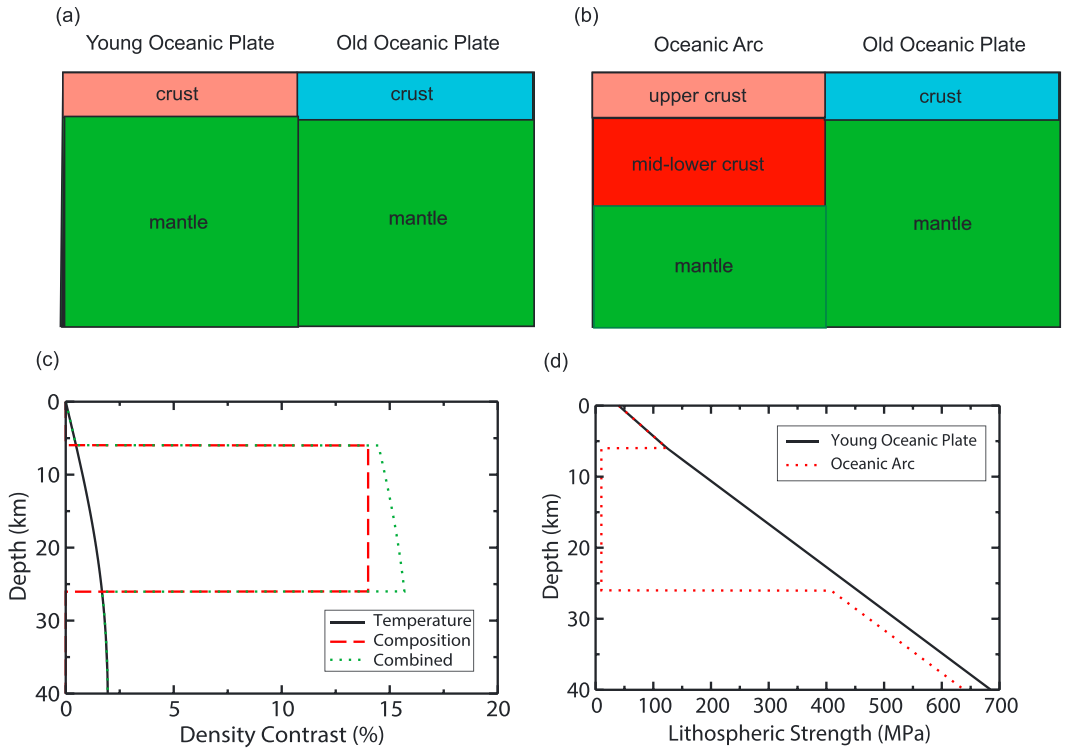

Figure 2. Different tectonic settings at the nascent plate boundary (a) without and (b) with a middle and lower arc crust. (c) Density contrast for different settings. The black solid curve shows the temperature effect due to the age offset at the transform fault, where the young and old oceanic plate ages are set 12 and 82 Ma, respectively. The red dashed curve shows the composition effect due to the buoyant middle and lower arc crust compared with the oceanic mantle. Here the mantle density is 3300 kg/m^3, and the average density for the middle and lower arc crust is 14% lower than the mantle density, i.e., 2838 kg/m^3. The green dotted line shows the combined effect of temperature and composition. (d) The lithospheric strength for the oceanic plate and for the oceanic arc with a weak middle and lower crust.

is consistent with joint gravity and seismic modeling of the relic arc immediately behind the Bonin Ridge in which the density at 20 km is ~12% lower than surrounding mantle in which the low density root extends to more than 30 km depth [*Kodaira et al.*, 2011]. Laboratory studies show that the existence of quartz and water may significantly reduce the lithospheric strength of the middle and lower crust for the continents [*Kohlstedt et al.*, 1995]. The continental crust is probably accreted from the arc volcanism [*Taylor and Mclennan*, 1995, and references therein]; therefore, the lithospheric strength of the arc may be similar to the continental crust, i.e., with a weak middle and lower crust (Figure 2d).

The combination of the reconstruction (Figure 1c), the recent seismic profiles in the Daito Ridge region, and the petrologic interpretation of the Mariana arc (Figure 2) suggest an important role of a weak middle and lower crust and a compositional gradient across the nascent boundary during SI. Isostatic arguments [*Niu et al.*, 2003] and geodynamic models [*Nikolaeva et al.*, 2010; *Sharples et al.*, 2014] have pointed to the importance of a compositional density contrasts between the continental and the oceanic lithosphere and the strength of the lithosphere in driving subduction evolution. Here we expand on recent geodynamic models [e.g., *Nikolaeva et al.*, 2010; *Leng and Gurnis*, 2011] to better appreciate the factors that may have lead to IBM initiation at 50 Ma and then to place IBM initiation within the context of other geologically constrained examples of subduction initiation.

2. Modeling Methods

As the elastic strength of the lithosphere and fault friction need to be overcome during subduction initiation [*McKenzie*, 1977; *Toth and Gurnis*, 1998], we use the finite element method to simulate the viscoelastoplastic properties of lithosphere and mantle. Our computational method follows from the 2-D Ellipsis approach [*Moresi et al.*, 2003] to solve the conservation equations of mass, momentum, and energy. We extend

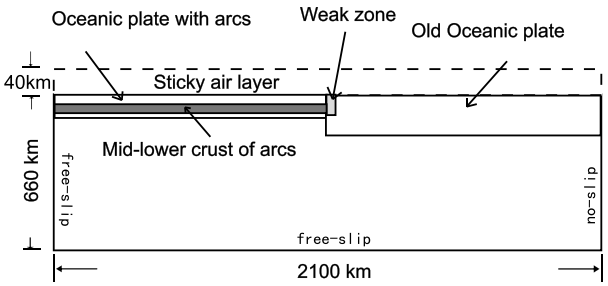

Figure 3. The model geometry used for this study. The top dashed line is the top boundary of the computational domain.

the viscoelastic and material tracking approach of the Ellipsis software into CitcomCU [*Zhong*, 2006] so as to exploit the later software's parallel processing capability. Lagrangian tracers are used to track the deformation history while material properties are advected with the velocities computed from the Eulerian grid. Please refer to *Moresi et al.* [2003] and *Leng and Gurnis* [2011] for specifics of the methodology. Our model is similar to *Leng and Gurnis* [2011] except that we are using a larger box and different boundary conditions (see below). The viscoelastoplastic method used is described only briefly here.

We use an incompressible Maxwell body to describe the viscoelasticity. Both viscous and elastic components contribute to the deformation rate:

$$\dot{\varepsilon}_{ij} = \frac{1}{2G}\dot{\tau}_{ij} + \frac{1}{2\eta}\tau_{ij}, \tag{1}$$

where $\dot{\varepsilon}_{ij}$ is strain rate, τ_{ij} is deviatoric stress, $\dot{\tau}_{ij}$ is time rate of change of deviatoric stress, η is dynamic viscosity, and G is shear modulus. i and j represent spatial indices.

Non-Newtonian viscosity is used [*Karato and Wu*, 1993], which is temperature dependent:

$$\eta = \eta_0 \left(\frac{\dot{\varepsilon}_{II}}{\dot{\varepsilon}_0}\right)^{\left(\frac{1}{n}-1\right)} \exp\left[\frac{E}{nR}\left(\frac{1}{T}-\frac{1}{T_0}\right)\right], \tag{2}$$

where the variables are the second invariant of the deviatoric strain rate tensor $\dot{\varepsilon}_{II}$, reference viscosity η_0, strain exponent n, reference strain rate $\dot{\varepsilon}_0$, gas constant R, activation energy E, reference temperatures T_0 (in Kelvin), and absolute temperature T. We also limit the viscosity range in our model between $\eta_{\min}$ and $\eta_{\max}$. The invariant model parameters used in the computations can be found in Table S1 in the supporting information.

We employ Drucker-Prager form for the material plasticity which gives the yield stress as follows:

$$\tau_y = \mu P + C, \tag{3}$$

where τ_y is the yield stress, P is pressure, μ is coefficient of friction, and C is cohesion which represents the material strength when no normal stress is applied. When plastic strain accumulates, mantle material may become weaker [*Poliakov and Buck*, 1998; *Buck and Poliakov*, 1998]. In our model, when accumulated plastic strain increases, μ and C both linearly decrease as follows:

$$\mu = \mu_0\left[1 - \min\left(1, \frac{\varepsilon_p}{\varepsilon_f}\right)\right], \tag{4}$$

$$C = C_f + (C_0 - C_f)\left[1 - \min\left(1, \frac{\varepsilon_p}{\varepsilon_f}\right)\right], \tag{5}$$

where the variables are the initial coefficient of friction μ_0, reference plastic strain ε_f, accumulated plastic strain ε_p, minimum cohesion C_f, and initial cohesion C_0. Such linear weakening mechanism stops when the accumulated plastic strain ε_p reaches ε_f.

Our model dimensions are 2100 km wide and 660 km deep (Figure 3). The depth of the box is larger than the existing models of SI [e.g., *Nikolaeva et al.*, 2010; *Leng and Gurnis*, 2011]. A 40 km thick "sticky air layer" (compressible, zero density with $\eta_{\min}$ as viscosity) is imposed above the lithosphere for a free surface simulation. Such a layer could be an important factor governing the emergence of single-sided subduction [*Crameri et al.*, 2012]. There are 257 × 129 grids in the horizontal and vertical directions, leading to a resolution of 8.2 km and 5.5 km in both directions. In every element, 16 tracers are initially deployed to track deformation and material properties. Isothermal boundary conditions are imposed at the top and bottom boundaries with fixed temperature at 0°C and T_0 = 1500°C, respectively. Lateral boundaries are insulating. A half-space cooling model is employed to

compute the initial temperature of the mantle [*Turcotte and Schubert*, 2002]. Free-slip conditions are applied to all the boundaries except for the right one, where no-slip conditions are applied.

The model domain is divided between an overriding and a subducting plate at the center of the box. Material properties are the same for these two plates except that we insert a middle and lower crust for the left oceanic plate with arcs (Figure 2b). For all cases, the age of the old oceanic plate is fixed at 82 Ma and the age of the overriding plate where the arc is located varies. The thickness of the upper crust for both plates is 7 km, with a density of 2800 kg/m^3. The thickness of the middle and lower crust is set as a variable model parameter. The density of the middle and lower crust is 14% lower than the averaged mantle density 3300 kg/m^3 (Figure 2c). Such a compositional density contrast, together with the thermal density contrast caused by the age offset between the two adjacent plates are the two major driving mechanism for subduction initiation (Figure 2c). Besides the driving forces, another critical factor affecting subduction initiation is the strength of the middle and lower crust. The plastic parameters μ_0, ε_f, C_0, and C_f are set as 0.5, 0.3, 40, and 0.6 MPa for the upper crust and mantle. For the middle and lower crust, we reduce μ_0 and C_0 to 0.0 and 10 MPa, to generate a weak layer. The initial yield stress computed from equation (3) for both plates are shown in Figure 2d. We also place a weak zone (17.5 by 17.5 km) at the plate interface (Figure 3), where μ_0, ε_f, C_0, and C_f are set as 0.0, 0.01, 0.6, and 0.6 MPa, respectively.

3. Results

We present results from 18 cases that vary the age offset and middle and lower crustal thickness to examine these parameters on subduction initiation with relic arcs. We first start from a case with the age offset across the place interface, $t_a = 70$ Ma and the middle and lower crust thickness $h_{lc} = 20$ km (Figures 4a and 4b). Within a few million years (Myr), the old oceanic plate starts foundering into the mantle. Strong mantle upwellings flush into the mantle wedge, which is accompanied by fast trench retreat and intense back-arc spreading (Figure 4b). This spontaneous subduction initiation is induced by the combination of thermal and compositional density anomalies between the arc and the old oceanic plate.

We then perform a series of computations (16 in total) by varying the thickness of the middle and lower arc crust between 16 and 28 km, and the age offset between 10 and 70 Ma (Figure 4a). We find that only with a large age offset and a thick arc middle and lower crust can subduction initiate spontaneously (Figure 4a). With a large t_a of 70 Ma across the plate interface, we observe spontaneous SI when h_{lc} exceeds 20 km. On the other hand, with a large h_{lc} of 28 km, we observe spontaneous SI when t_a is larger than 50 Ma (Figure 4a). These results show that when an oceanic arc is located adjacent to a plate interface, it provides a favorable tectonic environment for spontaneous subduction initiation.

We then compute two additional cases to highlight key parameters. On the one hand, if t_a is as large as 70 Ma, but with no arc middle and lower crust ($h_{lc} = 0$), no spontaneous SI is observed after a long period (i.e., more than 20 Myr) (Figures 4a and 4c). This suggests that at a normal transform fault which separates two oceanic plates, spontaneous SI is difficult even if there exist large age offsets (i.e., strong thermal density anomaly), consistent with previous results that strong plate convergence is a prerequisite to induce SI in such an environment [*Toth and Gurnis*, 1998; *Hall et al*., 2003; *Leng and Gurnis*, 2011]. On the other hand, if h_{lc} is 28 km, but with no age offset ($t_a = 0$), no spontaneous SI was observed (Figures 4a and 4d). This shows that the compositional density contrast alone is not sufficient to induce spontaneous SI. At passive margins, the continental plate typically has a thick middle and lower crust compared with the adjacent oceanic plate (e.g., the passive margins between the Atlantic Ocean and the North America) and therefore produces strong compositional density anomalies. But the continental plate is typically older or at a similar age compared with the adjacent oceanic lithosphere. Thus, the thermal density anomalies at the passive margins do not provide sufficient driving forces for inducing spontaneous SI. It actually provides resistance forces for SI if the continental plate is older than the oceanic plate.

Our results suggest that there are two possible routes for triggering spontaneous SI for an oceanic arc setting, as shown by the blue and red arrows in Figure 4a. First, when the middle and lower crust thickness is large, a thermal rejuvenation of the overriding arc plate, which significantly increases the age offset, may induce spontaneous SI (blue arrow in Figure 4a). Such a thermal rejuvenation may be caused by large-scale mantle upwellings, plume activity [e.g., *Burov and Cloetingh*, 2010], or plate stretching of divergence in an orthogonal

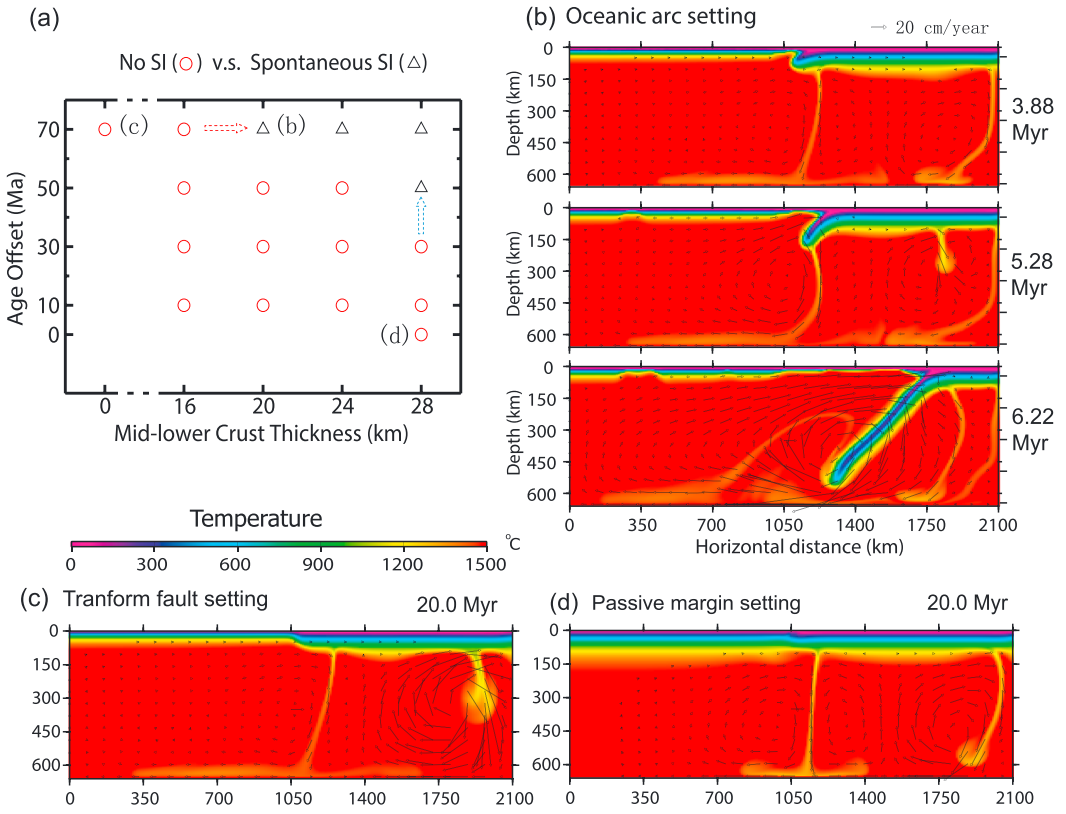

Figure 4. Numerical modeling results for subduction initiation (SI) adjacent to oceanic arcs. (a) Model results in the domain of crustal thickness and age offset showing the transition from no spontaneous SI (red circles) to spontaneous SI (black triangles). Letters b, c, and d indicate the cases whose temperature and velocity fields are shown in Figures 4b–4d. (b) A case with both a thick middle and lower crust and a large age offset which together lead to a spontaneous SI within several million years. (c) A case with only an age offset effect corresponding to a transform fault setting. (d) A case with only crustal composition corresponding to a passive margin setting. The blue dashed arrow shows the transition caused by thermal rejuvenation which increases the age offset. The red dashed arrow shows the transition caused by crustal thickening.

direction to the new boundary. Second, when the age offset is large, an increased middle and lower crust thickness may induce spontaneous SI (red arrow in Figure 4a). At active arcs, the arc crust is continuously thickened by the cumulative effect of volcanism. When the arc crust becomes sufficiently thick, new spontaneous SI is triggered at the arc margins of old subduction zones.

The lithospheric strength of the middle and lower arc crust also plays an important role in promoting spontaneous SI. If we do not reduce μ_0 and C_0 for the middle and lower crust (see Figure 2d), spontaneous SI is not observed within the parameter space we explored. We propose that a weak middle and lower crust increases the possibility of crustal flow and decouples the upper crust and the upper mantle and therefore leads to the back-arc spreading process, which may strongly enhance trench retreat and slab foundering.

4. Discussion

The new computational models, although extensions to existing studies [*Nikolaeva et al.*, 2010; *Leng and Gurnis*, 2011], provide the avenue to evaluate the different geodynamic factors that are important for SI in light of the recent IBM drilling. The models also help to place other observations in a clearer framework. Specifically, the new "phase diagram" (Figure 4a) places the passive margins and fracture zones into a framework that allows us to better understand why SI is favorable in some tectonic environments but not in others. From theoretical analysis, the transform faults are the most favorable places for SI [*Mueller and Phillips*, 1991]. But previous computational studies indicate that plate convergence is typically required for inducing SI at the transform faults. Here with our new models, we show that if additional driving forces from compositional contrasts are supplied through the presence of relic arcs, spontaneous SI becomes possible at transform faults.

The models help us to better understand the role different factors played in the initiation of the IBM arc. The relic arcs within the northern part of the West Philippine Sea Plate are clearly Cretaceous in age (110–120 Ma) and presumably turned off as active arcs around 110 Ma [*Seton et al*., 2012]. The subsequent subsidence of the arcs during the Eocene [*Mizuno et al*., 1978] is consistent with prolonged stability. Despite the strong compositional gradients there is no evidence for a new subduction zone between 110 and 50 Ma. The extensional event that pulled the Amami Plateau away from the Daito Ridge as well as the formation of the Amami Sankaku Basin (Figure 1) in what is now a N-S direction is critical for the onset of SI. We hypothesize that this event thermally rejuvenated and created new oceanic crust as indicated by the 60–40 Ma thermal age of the ASB [*Expedition 351 Scientists*, 2014]. The thermal age, with the microfossils that immediately overlay the ASB basement, bounds the basement age to 57–50 Ma [*Expedition 351 Scientists*, 2014]. This implies that the overlaying plate was in the range of 0 to 7 Myr in age at 50 Ma. Also at 50 Ma, the adjacent Pacific Plate was in the range of 50–70 Myr old [*Hall et al*., 2003; *Seton et al*., 2012]. Such a young overriding plate age and a large age offset between the two plates are consistent with our model setup. If the Pacific Plate abutted the relic arcs, this would have led to spontaneous subduction initiation within several million years (Figure 4a). We do not know if this SI event predates or postdates the change in Pacific Plate motion at about 50 Ma [*Sharp and Clague*, 2006]. If the change in plate motion predates the initiation, then compression adjacent to the relic ridges could also have contributed to the initiation [*Gurnis et al*., 2004]. Although coarse-grained clastic sediments are interbedded with muds just above the basement at Site U1438 in the ASB [*Expedition 351 Scientists*, 2014], we do not yet know if these were shed from new volcanic constructs or uplifted basement during subduction initiation [*Arculus et al*., 2015].

If a new subduction event was responsible for the extension at 50 Ma within the ASB region, then the slab presumably would have also injected fluids into the mantle beneath the relic arc and intervening pieces of oceanic crust. If that were the case, then this would have led to some hydration of the middle and lower crust. Any quartzite in the arc crust would then have had a substantial reduction in its strength [e.g., *Kohlstedt et al*., 1995]. Together, the lower density and lower strength could facilitate SI. We find this possibility interesting in light of earlier discussions of the initiation of subduction. *Regenauer-Lieb et al*. [2001] suggested that hydration of the mantle and lower lithosphere must precede initiation of subduction. Although these authors were applying the hydration scenario to a passive margin (a much more challenging setting for SI, see below), we find that the concept is also applicable to a relic arc setting.

Another tectonic locus with a major compositional gradient that has long been thought to be important for subduction initiation is a passive margin. Force analysis indicates that it is extremely difficult to initiate subduction at old passive continental margins because of the large driving forces required to overcome strong shear coupling and plate bending [*Mueller and Phillips*, 1991]. *Nikolaeva et al*. [2010] modeled the effects of chemical density contrasts between continental and oceanic plates and a ductile lower continental crust on promoting SI at passive margins. They predicted that Brazil's Atlantic margin may well evolve into an active subduction zone [*Nikolaeva et al*., 2011]. Our models do not try to model the passive margin setting in detail. For example, the actual thickness of the continental lithosphere can be much thicker than in our models. But the new results suggest that transform faults located beside relic arcs are the much more favorable places for spontaneous SI compared with passive margins. This is because the thermal density contrast at the relic arcs acts as one of the major driving forces, whereas it becomes a resisting force at passive margins. Our results, with the relic arcs as a key factor, can successfully explain the occurrence of SI at IBM and the stability of passive margins around the Atlantic Ocean.

Our models are computed in a 2-D geometry that ignores possible thermal, compositional, or structural heterogeneities along the trench. Such heterogeneities may lead to complex geodynamic behaviors during subduction initiation [*Marques et al*., 2014]. For example, will the spontaneous SI occur at approximately the same time along the whole trench? Or is it time dependent? These questions deserve further investigations with fully 3-D geometry.

Acknowledgments
This work is supported by the National Natural Science Foundation of China (91114203 and 41422402), National Science Foundation (EAR-1247022), and a postexpedition award for IODP Expedition 351. Wei Leng is also partially supported by the Fundamental Research Funds for the Central Universities (WK2080000053).

The Editor thanks Margarete Jadamec and an anonymous reviewer for their assistance in evaluating this paper.

References

Arculus, R. J., et al. (2015), A record of spontaneous subduction initiation in the Izu-Bonin-Mariana arc, *Nat. Geosci.*, *8*, 728–733, doi:10.1038/ngeo2515.

Buck, W. R., and A. N. B. Poliakov (1998), Abyssal hills formed by stretching oceanic lithosphere, *Nature*, *392*, 272–275.

Burov, E., and S. Cloetingh (2010), Plume-like upper mantle instabilities drive subduction initiation, *Geophys. Res. Lett.*, *37*, L03309, doi:10.1029/2009GL041535.

Cosca, M. A., R. J. Arculus, J. A. Pearce, and J. G. Mitchell (1998), 40Ar/39Ar and K-Ar geochronological age constraints for the inception and early evolution of the Izu-Bonin-Mariana arc system, *Isl. Arc*, *7*, 579–595.

Crameri, F., P. Tackley, I. Meilick, T. Gerya, and B. Kaus (2012), A free plate surface and weak oceanic crust produce single-sided subduction on Earth, *Geophys. Res. Lett.*, *39*, L03306, doi:10.1029/2011GL050046.
Deschamps, A., and S. Lallemand (2002), The West Philippine Basin: An Eocene to early Oligocene back arc basin opened between two opposed subduction zones, *J. Geophys. Res.*, *107*(B12), 2322, doi:10.1029/2001JB001706.
Expedition 351 Scientists (2014), Izu-Bonin-Mariana arc origins: Continental crust formation at an intra-oceanic arc: Foundation inception, and early evolution International Ocean Discovery Program Preliminary Report, 351, doi:10.14379/iodp.pr.351.2014.
Forsyth, D., and S. Uyeda (1975), On the relative importance of the driving forces of plate motion, *Geophys. J. R. Astron. Soc.*, *43*, 163–200.
Gurnis, M., C. Hall, and L. Lavier (2004), Evolving force balance during incipient subduction, *Geochem. Geophys. Geosyst.*, *5*, Q07001, doi:10.1029/2003GC000681.
Hager, B. H., and R. J. O'Connell (1981), A simple global model of plate dynamics and mantle convection, *J. Geophys. Res.*, *86*, 4843–4867, doi:10.1029/JB086iB06p04843.
Hall, C. E., M. Gurnis, M. Sdrolias, L. L. Lavier, and R. D. Muller (2003), Catastrophic initiation of subduction following forced convergence across fracture zones, *Earth Planet. Sci. Lett.*, *212*, 15–30, doi:10.1016/S0012-821X(03)00242-5.
Hickey-Vargas, R. (2005), Basalt and tonalite from the Amami Plateau, northern West Philippine Basin: New Early Cretaceous ages and geochemical results and their petrologic and tectonic implications, *Isl. Arc*, *14*, 653–665.
Ishizuka, O., K. Tani, M. K. Reagan, K. Kanayama, S. Umino, Y. Harigane, I. Sakamoto, Y. Miyajima, M. Yuasa, and D. J. Dunkley (2011a), The timescales of subduction initiation and subsequent evolution of an oceanic island arc, *Earth Planet. Sci. Lett.*, *306*, 229–240.
Ishizuka, O., R. N. Taylor, M. Yuasa, and Y. Ohara (2011b), Making and breaking an island arc: A new perspective from the Oligocene Kyushu-Palau arc, Philippine Sea, *Geochem. Geophys. Geosyst.*, *12*, Q05005, doi:10.1029/2010GC003440.
Karato, S. I., and P. Wu (1993), Rheology of the upper mantle: A synthesis, *Science*, *260*, 771–778.
Kitamura, K., M. Ishikawa, and M. Arima (2003), Petrological model of the northern Izu-Bonin-Mariana arc crust: Constraints from high-pressure measurements of elastic wave velocities of the Tanzawa plutonic rocks, central Japan, *Tectonophysics*, *371*, 213–221.
Kodaira, S., T. Fujiwara, N. Noguchi, and N. Takahashi (2011), Structural variation of the Bonin ridge revealed by modeling of seismic and gravity data, *Earth Planets Space*, *63*, 963–973, doi:10.5047/eps.2011.06.036.
Kohlstedt, D. L., B. Evans, and S. J. Mackwell (1995), Strength of the lithosphere: Constraints imposed by laboratory experiments, *J. Geophys. Res.*, *100*(B9), 17,587–17,602, doi:10.1029/95JB01460.
Leng, W., and M. Gurnis (2011), Dynamics of subduction initiation with different evolutionary pathways, *Geochem. Geophys. Geosyst.*, *12*, Q12018, doi:10.1029/2011GC003877.
Marques, F. O., F. R. Cabral, T. V. Gerya, G. Zhu, and D. A. May (2014), Subduction initiates at straight passive margins, *Geology*, *42*(4), 331–334.
McKenzie, D. P. (1977), The initiation of trenches: A finite amplitude instability, in *Island Arcs, Deep Sea Trenches, and Back-Arc Basins*, *Maurice Ewing Ser.*, vol. 1, edited by M. Talwani and W. C. Pitman III, pp. 57–61, AGU, Washington, D. C.
Mizuno, A., Y. Okuda, S. Nagumo, H. Kagami, and N. Nasu (1978), Subsidence of the Daito Ridge and associated basins, North Philippine Sea, in *Geological and Geophysical Investigations of Continental Margins*, *AAPG Mem.*, vol. 29, edited by J. S. Watkins et al., pp. 239–243, American Association, of Petroleum Geologists, Tulsa, Okla.
Moresi, L., F. Dufour, and H. B. Muhlhaus (2003), A Lagrangian integration point finite element method for large deformation modeling of viscoelastic geomaterials, *J. Comp. Phys.*, *184*, 476–497.
Mueller, S., and R. J. Phillips (1991), On the initiation of subduction, *J. Geophys. Res.*, *96*, 651–665, doi:10.1029/90JB02237.
Nikolaeva, K., T. V. Gerya, and F. O. Marques (2010), Subduction initiation at passive margins: Numerical modeling, *J. Geophys. Res.*, *115*, B03406, doi:10.1029/2009JB006549.
Nikolaeva, K., T. V. Gerya, and F. O. Marques (2011), Numerical analysis of subduction initiation risk along the Atlantic American passive margins, *Geology*, *39*, 463–466, doi:10.1130/G31972.1.
Nishizawa, A., K. Kaneda, Y. Katagiri, and M. Oikawa (2014), Wide-angle refraction experiments in the Daito Ridges region at the northwestern end of the Philippine Sea plate, *Earth Planets Space*, *66*, 1–16.
Niu, Y., M. J. O'Hara, and J. A. Pearce (2003), Initiation of subduction zones as a consequence of lateral compositional buoyancy contrast within the lithosphere: A petrological perspective, *J. Petrol.*, *44*, 851–866.
Poliakov, A. N. B., and W. R. Buck (1998), Mechanics of stretching elastic-plastic-viscous layers: Applications to slow-spreading mid-ocean ridges, in *Faulting and Magmatism at Mid-Ocean Ridges*, *Geophys. Monogr. Ser.*, vol. 106, edited by W. R. Buck et al., pp. 305–325, AGU, Washington, D. C.
Regenauer-Lieb, K., D. A. Yuen, and J. Branlund (2001), The initiation of subduction: Criticality by addition of water?, *Science*, *294*, 578–580.
Ryan, W. B. F., et al. (2009), Global multi-resolution topography synthesis, *Geochem. Geophys. Geosyst.*, *10*, Q03014, doi:10.1029/2008GC002332.
Seton, M., et al. (2012), Global continental and ocean basin reconstructions since 200 Ma, *Earth Sci. Rev.*, *113*, 212–270.
Sharp, W. D., and D. A. Clague (2006), 50-Ma initiation of Hawaiian-Emperor bend records major change in Pacific Plate motion, *Science*, *313*, 1281–1284.
Sharples, W., M. A. Jadamec, L. N. Moresi, and F. A. Capitanio (2014), Overriding plate controls on subduction evolution, *J. Geophys. Res. Solid Earth*, *119*, 6684–6704, doi:10.1002/2014JB011163.
Smith, W. H. F., and D. T. Sandwell (1997), Global seafloor topography from satellite altimetry and ship depth soundings, *Science*, *277*, 1957–1962.
Stern, R. J., and S. H. Bloomer (1992), Subduction zone infancy: Examples from the Eocene Izu-Bonin-Mariana and Jurassic California arcs, *Geol. Soc. Am. Bull.*, *104*, 1621–1636.
Takahashi, N., S. Kodaira, S. L. Klemperer, Y. Tatsumi, Y. Kaneda, and K. Suyehiro (2007), Crustal structure and evolution of the Mariana intra-oceanic island arc, *Geology*, *35*, 203–206.
Taylor, B., and A. M. Goodliffe (2004), The West Philippine Basin and the initiation of subduction, revisited, *Geophys. Res. Lett.*, *31*, L12602, doi:10.1029/2004GL020136.
Taylor, S. R., and S. M. Mclennan (1995), The geochemical evolution of the continental crust, *Rev. Geophys.*, *33*(2), 241–265, doi:10.1029/95RG00262.
Toth, J., and M. Gurnis (1998), Dynamics of subduction initiation at pre-existing fault zones, *J. Geophys. Res.*, *103*, 18,053–18,067, doi:10.1029/98JB01076.
Turcotte, D. L., and G. Schubert (2002), *Geodynamics*, 2nd ed., 456 pp., Cambridge Univ. Press, New York.
Zhong, S. (2006), Constraints on thermochemical convection of the mantle from plume heat flux, plume excess temperature, and upper mantle temperature, *J. Geophys. Res.*, *111*, B04409, doi:10.1029/2005JB003972.